Complexity and Floquet dynamics: Nonequilibrium Ising phase transitions

Giancarlo Camilo[*]
International Institute of Physics, Universidade Federal do Rio Grande do Norte, Campus Universitário, Lagoa Nova, Natal, Rio Grande do Norte 59078-970, Brazil

Daniel Teixeira[†]
Institute of Physics, University of São Paulo, São Paulo 05314-970, Brazil

(Received 4 September 2020; accepted 23 October 2020; published 9 November 2020)

We study the time-dependent circuit complexity of the periodically driven transverse field Ising model using Nielsen's geometric approach. In the high-frequency driving limit the system is known to exhibit nonequilibrium phase transitions governed by the amplitude of the driving field. We analytically compute the complexity in this regime and show that it clearly distinguishes between the different phases, exhibiting a universal linear behavior at early times. We also evaluate the time-averaged complexity, provide evidence of nonanalytic behavior at the critical points, and discuss its origin. Finally, we comment on the freezing of quantum dynamics at specific configurations and on the use of complexity as a tool to understand quantum phase transitions in Floquet systems.

DOI: 10.1103/PhysRevB.102.174304

I. INTRODUCTION

Understanding the organizing principles underlying the nonequilibrium dynamics of quantum many-body systems is of key importance for the development of new quantum materials. The concept of universality, which provides a unified description of equilibrium critical phenomena, is not well understood for systems far from equilibrium. In the case of adiabatic dynamics the so-called Kibble-Zurek mechanism and its quantum extension can provide some insights into the breakdown of adiabaticity close to a quantum phase transition (QPT) point and the associated scaling behavior of the excitation density of defects [1–5], which opened a venue for the analysis of universal features in nonequilibrium QPTs. The preclusion of adiabatically connecting states belonging to different quantum phases can be given a geometric interpretation as a diverging curvature with the introduction of a metric on the Hilbert space [6]. This geometric paradigm is part of an ongoing effort in the last two decades to employ concepts and tools from quantum information science to improve our understanding of quantum many-body physics. This approach has led to remarkable progresses, such as the discovery of topologically ordered states and of the critical behavior of entanglement close to a QPT [7,8] (see [9] for a review).

As part of this effort, [10–12] proposed to characterize QPTs, including topological ones, using a geometric notion of circuit complexity introduced by Nielsen [13,14]. Inspired by its computer science analog, this object quantifies how difficult it is to construct a particular unitary operator that maps between a pair of given reference and target states, i.e., the minimum number of basic operations needed to implement this task. With an appropriate definition of depth functional associated with each circuit, the space of allowed unitaries acquires a Riemannian structure and the problem of finding the optimal circuit reduces to finding minimal geodesics in this geometry. Nielsen's complexity has recently also attracted a lot of interest from the high-energy physics community due to conjectured connections with black hole properties within the scope of the holographic duality [15–19].

A major difficulty to unravel universal nonequilibrium properties independent of specific models comes from the variety of ways in which a system can be put away from equilibrium. Perhaps the simplest and one of the most studied among these nonequilibrium protocols is that of a quantum quench, where a parameter of the Hamiltonian is suddenly changed and the system is left to evolve under the new Hamiltonian [20,21]. This also includes the study of the quench dynamics of circuit complexity [10,11,22–25]. Here we propose to go a step further in the endeavor of using circuit complexity as a tool to understand the dynamics of quantum many-body systems and explore a different nonequilibrium protocol corresponding to the periodic driving of many-body systems. These so-called Floquet systems can be experimentally realized with ultracold quantum gases in optical lattices (see [26,27] for a review of theoretical and experimental results) and give rise to several exotic phenomena such as dynamical localization, Floquet topological insulators, and driving-induced phase transitions [26–30].

We shall focus on the Ising model under periodic driving of the transverse field [31–34]. The model can be solved analytically in the fast-driving limit, where it is effectively described by a time-independent Hamiltonian and it displays quantum phase transitions of a nonequilibrium nature controlled by the transverse field amplitudes. It also exhibits the phenomenon of dynamic localization [35], where the time evolution gets frozen in the initial state as a consequence of a many-body

[*]gcamilo@iip.ufrn.br
[†]dteixeira@usp.br

version of the coherent destruction of tunneling (CDT) [36] that occurs in each momentum sector of the Hilbert space. CDT has been observed experimentally, and it is particularly important for quantum dynamics control [37–39].

In this setup, we compute the circuit complexity of the instantaneous time-evolved state and argue that it can be used to characterize these nonequilibrium phase transitions, showing that its time average exhibits nonanalytic behavior at the critical points. We also unveil a universal linear behavior at early times and show that the CDT phenomenon is naturally diagnosed by points of vanishing complexity. Our work takes to the next level the connection between circuit complexity and quantum phase transitions, opening the route for periodically driven systems and dynamical phase transitions.

II. THE DRIVEN TRANSVERSE FIELD ISING MODEL

We consider a periodically driven transverse field Ising model (TFIM) described by the Hamiltonian

$$H(t) = -J\sum_{i=1}^{L}\sigma_i^z\sigma_{i+1}^z - g(t)\sum_{i=1}^{L}\sigma_i^x, \tag{1}$$

where σ_i^α are Pauli matrices at the ith lattice site, $J>0$ is the exchange coupling, and $g(t) = g_0 + g_1\cos\Omega t$ is the transverse field, made of a constant contribution g_0 and a monochromatic driving with frequency Ω. Here we assume a closed lattice with periodic boundary conditions $\sigma_{L+1}^\alpha \equiv \sigma_1^\alpha$ and restrict ourselves to even L. The $\mathbb{Z}_2$ symmetry of the model is implemented by the parity operator $\mathcal{P} = \prod_{i=1}^{L}\sigma_i^x$, resulting in a decomposition of the Hilbert space into a direct sum of parity-odd ($\mathcal{P}=-1$) or -even ($\mathcal{P}=+1$) subspaces [40], each of dimension 2^{L-1},the so-called Ramond and Neveu-Schwarz (NS) sectors, respectively. We shall focus on only the NS sector.

In terms of Jordan-Wigner fermions c_j, after the discrete Fourier transform, $c_j = \frac{e^{-i\pi/4}}{\sqrt{L}}\sum_{k\in \mathrm{BZ}} c_k e^{ikj}$, the Hamiltonian can be written as $H(t) = \sum_{k>0} H_k(t)$, with

$$\begin{aligned} H_k(t) &= [2g(t)-\omega_k](c_k^\dagger c_k + c_{-k}^\dagger c_{-k}) \\ &\quad + \Delta_k(c_k^\dagger c_{-k}^\dagger + c_{-k}c_k) - \omega_k, \end{aligned} \tag{2}$$

where $\omega_k = 2J\cos k$, $\Delta_k = 2J\sin k$, and we have neglected the trivial contribution $-2Lg(t)$. The momenta are constrained to the first Brillouin zone, $\mathrm{BZ} = \{\pm\frac{\pi}{L}, \pm\frac{3\pi}{L}, \ldots, \pm\frac{(L-1)\pi}{L}\}$, by the antiperiodic boundary condition satisfied by c_j in the NS sector.

Since the Hamiltonian conserves momentum and parity, the state of a system initialized in a ground state of the undriven model will acquire at any time t the following form [3,31,41]:

$$|\psi(t)\rangle = \bigotimes_{k>0}[u_k(t)\,|1_{-k}1_k\rangle + v_k(t)\,|0_{-k}0_k\rangle]; \tag{3}$$

that is, for each k the dynamics is restricted to the two-level Nambu subspace spanned by $\{|0_{-k}0_k\rangle, |1_{-k}1_k\rangle\}$. One can unify the coefficients into the spinor $\Psi_k(t) \equiv [u_k(t)\ v_k(t)]^\intercal$, which obeys Schrödinger's equation generated by the Bogoliubov–de Gennes (BdG) Hamiltonian (2), such that the dynamics of each momentum mode takes the form of a driven two-level system. In terms of $\mathfrak{u}(2)$ generators, one has

$$H_k(t) = [2g(t)-\omega_k]\,\sigma_k^z + \Delta_k\,\sigma_k^x - \omega_k\,\mathbb{1}_k. \tag{4}$$

According to the Floquet theorem, the solution can be written as

$$\Psi_k(t) = \sum_{\lambda=\pm} A_\lambda e^{i\,\varepsilon_k^{(\lambda)}t}\,\Phi_k^{(\lambda)}(t), \tag{5}$$

where the Floquet modes $\Phi_k^{(\pm)}(t) = \Phi_k^{(\pm)}(t + 2\pi\,\Omega^{-1})$ are periodic with the same period as the external driving and satisfy the time-independent Schrödinger equation for the Floquet Hamiltonian $\mathcal{H}_k \equiv H_k(t) - i\,\partial_t$. The Floquet quasienergies $\varepsilon_k^{(\lambda)}$ are defined only modulo Ω since $e^{i\,m\Omega t}\,\Phi_k^{(\pm)}(t)$ for any $m\in\mathbb{Z}$ obviously defines another Floquet mode with quasienergy shifted by $m\Omega$, meaning, in particular, that the driven system admits no notion of a ground state. For simplicity, in the following section we discuss exact solutions in the limit of high Ω following [34,42]. Generalizations to low Ω are possible using the full exact solution [43] or the $1/\Omega$ expansion of [44].

A. High-frequency driving approximation

It will be convenient to split the constant part of the transverse field as $g_0 = \delta g_0 + \tilde{g}_0$, where $\tilde{g}_0$ is a resonant value (to be determined) and $\delta g_0 \equiv g_0 - \tilde{g}_0$ is a detuning measuring the distance to this resonance.

The dynamics can then be solved by going to a rotating frame tweaked to the driving field $g(t)$ through a unitary transformation $\mathcal{R}_k(t)$. First, we split $H_k(t) = H_k^0(t) + H_k^1$, with $H_k^0(t) \equiv 2(\tilde{g}_0 + g_1\cos\Omega t)\,\sigma_k^z$ and $H_k^1 \equiv \Delta_k\,\sigma_k^x + (2\delta g_0 - \omega_k)\,\sigma_k^z - \omega_k\,\mathbb{1}_k$, and go to the interaction picture with H_k^1 being the interaction Hamiltonian. The desired transformation is the time evolution operator associated with $H_k^0(t)$, namely,

$$\mathcal{R}_k(t) = e^{-\frac{i}{2}\alpha(t)\sigma_k^z}, \quad \alpha(t) = 4\tilde{g}_0 t + \frac{4g_1}{\Omega}\sin\Omega t. \tag{6}$$

The rotated Hamiltonian $\tilde{H}_k(t) \equiv \mathcal{R}_k^\dagger(t)H_k(t)\mathcal{R}_k(t) = H_k^0(t) + \tilde{H}_k^1(t)$ has the same free contribution and a rotating part given by

$$\tilde{H}_k^1(t) = \begin{pmatrix} 2\delta g_0 - 2\omega_k & \Delta_k e^{i\,\alpha(t)} \\ \Delta_k e^{-i\,\alpha(t)} & -2\delta g_0 \end{pmatrix}. \tag{7}$$

States $|\psi(t)\rangle_k$ whose dynamics is governed by (4) are mapped to rotated states $|\tilde{\psi}(t)\rangle_k = \mathcal{R}_k^\dagger(t)\,|\psi(t)\rangle_k$ with Schrödinger time evolution dictated by (7). The full rotated Hamiltonian $\tilde{H}^1(t) \equiv \sum_{k>0}\tilde{H}_k^1(t)$ in terms of the original spins contains all possible nearest-neighbor free-fermion terms σ_i^x, $\sigma_i^z\sigma_{i+1}^z$, $\sigma_i^y\sigma_{i+1}^y$, $\sigma_i^z\sigma_{i+1}^y$, $\sigma_i^y\sigma_{i+1}^z$ [34].

In order to determine the resonance condition, we first make use of the Jacobi-Anger expansion $e^{i\,z\sin\Omega t} = \sum_{n\in\mathbb{Z}}\mathcal{J}_n(z)\exp(i\,n\Omega t)$, where $\mathcal{J}_n(z)$ are Bessel functions of the first kind, to rewrite (7) in the form $\tilde{H}_k^1(t) = \sum_{n\in\mathbb{Z}}\tilde{h}^{(n)}e^{i(4\tilde{g}_0 - n\Omega)t}$ for some $\tilde{h}^{(n)}$. Then, the high-frequency approximation (sometimes referred as the rotating wave approximation) is performed assuming that all the terms in the summation oscillate wildly and can be neglected with respect

to a single resonant term given by

$$\tilde{g}_0^{(\ell)} = \ell\frac{\Omega}{4}, \quad \ell \in \mathbb{Z}. \tag{8}$$

The corresponding detuning parameter will be denoted by $\delta g_0^{(\ell)} = g_0 - \tilde{g}_0^{(\ell)}$. As a result, the effective Hamiltonian describing the dynamics of the system at the ℓth resonance becomes time independent.

In terms of the original spins, the full rotating frame Hamiltonian $\tilde{H}^{1(\ell)} = \sum_{k>0} \tilde{H}_k^{1(\ell)}$ takes the form

$$\tilde{H}^{1(\ell)} = -\sum_{j=1}^{L}\left[\delta g_0^{(\ell)}\sigma_j^x + J_+^{(\ell)}\sigma_j^z\sigma_{j+1}^z + J_-^{(\ell)}\sigma_j^y\sigma_{j+1}^y\right], \tag{9}$$

with $J_\pm^{(\ell)} \equiv \frac{J}{2}(1 \pm \gamma^{(\ell)})$ and

$$\gamma^{(\ell)} \equiv (-1)^\ell \mathcal{J}_\ell\left(\frac{4g_1}{\Omega}\right). \tag{10}$$

This is unitarily equivalent to the familiar transverse XY chain with the anisotropy parameter $\gamma^{(\ell)}$ [40,45]. The nontrivial dependence of $\gamma^{(\ell)}$ on ℓ, Ω, g_1 already anticipates the influence of the driving on the critical behavior of the system, which will be confirmed in the next section. Near the resonance there is pure coupling between the two-level system basis states at $\min_k |\omega_k|$, with oscillation frequency given by $\omega_{\text{eff}} = J|\gamma^{(\ell)}|$, indicating that this large-Ω approximation remains valid as long as $\delta g_0^{(\ell)}, \omega_{\text{eff}} \ll \Omega$.

B. Nonequilibrium QPTs in the rotating frame

The XY model (9) describing the high-Ω dynamics in the rotating frame is exactly solvable via Jordan-Wigner and discrete Fourier transforms following closely the discussion for the TFIM in Sec. II. The Bogoliubov angle $\vartheta_{k,\ell}$ defined by

$$\tan(2\vartheta_{k,\ell}) = \frac{\Delta_k\,\gamma^{(\ell)}}{2\delta g_0^{(\ell)} - \omega_k} \tag{11}$$

diagonalizes the corresponding BdG Hamiltonian to the free-fermion form $\tilde{H}^{1(\ell)} = \sum_{k>0} \epsilon_{k,\ell}(b_k^\dagger b_k - \frac{1}{2})$, with

$$\epsilon_{k,\ell} = \sqrt{\left(2\delta g_0^{(\ell)} - \omega_k\right)^2 + (\Delta_k\,\gamma^{(\ell)})^2}. \tag{12}$$

The positive- and negative-energy eigenstates, with eigenvalues $\epsilon_{k,\ell}^{\pm} = -\omega_k \pm \epsilon_{k,\ell}$, are $\phi_{k,+}^{(\ell)} = (\cos\vartheta_{k,\ell} \;\; -\sin\vartheta_{k,\ell})^\intercal$ and $\phi_{k,-}^{(\ell)} = (\sin\vartheta_{k,\ell} \;\; \cos\vartheta_{k,\ell})^\intercal$.

The model is known to present two critical lines: an Ising-like QPT between a ferromagnetic and a paramagnetic (PM) phase at $|\delta g_0^{(\ell)}| = J$ and an anisotropic QPT at $\gamma^{(\ell)} = 0$ (provided that $|\delta g_0^{(\ell)}| < J$) between two distinct phases with ferromagnetic order along the y direction (FMY, for $\gamma^{(\ell)} < 0$) or along the z direction (FMZ, for $\gamma^{(\ell)} > 0$). For a given ℓ, the former defines a pair of lines $\delta g_0^{(\ell)} = \pm J$, while the latter corresponds to an infinite family of critical lines, one for each zero of $\mathcal{J}_\ell(z)$. The phase diagram as a function of the transverse field strengths g_0, g_1 for fixed (and large) Ω is illustrated in Fig. 1. The FMY-FMZ transition lines are almost evenly spaced (except for the first few) since the sequence $\{z_{i+1} - z_i\}_{i\in\mathbb{Z}^+}$ of differences between two subsequent Bessel zeros converges very quickly to the constant value π, as seen intuitively from the asymptotic behavior $\mathcal{J}_\ell(z) \approx \sqrt{\frac{2}{\pi z}}\cos[z - (2\ell+1)\frac{\pi}{4}]$ at $z \gg \ell$. Note that in the special case $\delta g_0^{(\ell)} = 0$, i.e., when g_0 is tuned exactly to the resonant value $g_0^{(\ell)}$, the transverse field in (9) disappears, and we are left with only the anisotropic transitions.

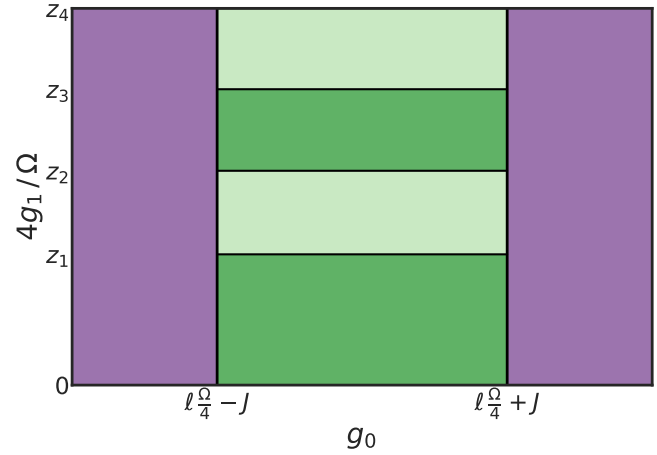

FIG. 1. Nonequilibrium phase diagram as a function of the transverse field strengths g_0, g_1 in the high-Ω regime. The phases are PM (purple), FMZ (dark green), and FMY (light green). Vertical and horizontal lines identify the Ising-like and anisotropic phase transitions, respectively. The latter are located at z_i, the ith root of $\mathcal{J}_\ell(z)$ ($\ell = 2$ is shown in the plot); the width $z_{i+1} - z_i$ quickly approaches π as i grows.

The horizontal lines in Fig. 1 occur at $\gamma^{(\ell)} = 0$, where $\omega_{\text{eff}} = 0$ forces the quantum tunneling between σ_k^z eigenstates to completely freeze. This phenomenon, known as coherent destruction of tunneling, occurs at every sector k once the driving amplitude is fine-tuned to one of the Bessel zeros, leading to a coherent suppression of the dynamics even at infinite L. We will show how this dynamic localization effect manifests in the circuit complexity in the next section.

C. Floquet modes and quasienergies

The Floquet modes that define a basis for the dynamics in the Schrödinger picture follow by applying $\mathcal{R}_k$ to the eigenstates of the XY Hamiltonian,

$$\Phi_{k,\pm}^{(\ell)}(t) \equiv e^{-i(\frac{\ell\Omega}{2}t + \frac{2g_1}{\Omega}\sin\Omega t)}\mathcal{R}_k^{(\ell)}(t)\,\phi_{k,\pm}^{(\ell)} \tag{13}$$

[the $U(1)$ phase is added for convenience], and correspond to quasienergies

$$\varepsilon_{k,\ell}^{\pm} \equiv -\omega_k \pm \epsilon_{k,\ell} + \frac{\ell\Omega}{2}. \tag{14}$$

Here we recall that there is an infinite family of Floquet modes, labeled by an integer m that is omitted here, corresponding to the rescaling $\Phi_{k,\pm}^{(\ell)}(t) \to e^{im\Omega t}\,\Phi_{k,\pm}^{(\ell)}(t)$ and shift $\varepsilon_{k,\ell}^{\pm} \to \varepsilon_{k,\ell}^{\pm} + m\Omega$. We choose the $m = 0$ representative without loss of generality.

Finally, the general solution (5) with initial condition $\Psi_k^{(\ell)}(0) \equiv [u_k^{(\ell)}(0)\; v_k^{(\ell)}(0)]^\intercal$ is completely determined due to the orthogonality of the Floquet modes by the coefficients $A_{k,\ell}^{\pm} \equiv \Psi_k^{(\ell)}(0)\,\phi_{k,\pm}^{(\ell)}$. We will focus on $\Psi_k^{(\ell)}(0) = (0\;1)^\intercal$, i.e.,

a system initialized in the paramagnetic state of the undriven model with all the spins aligned along the x direction, $\bigotimes_{k>0}|0_k 0_{-k}\rangle$, corresponding to $A^+_{k,\ell} = -\sin\vartheta_{k,\ell}$ and $A^-_{k,\ell} = \cos\vartheta_{k,\ell}$. In terms of the spinor components introduced in (3), the explicit solution $\Psi^{(\ell)}_k(t)$ reads (up to a global phase $e^{-i\varepsilon^-_{k,\ell}t}$)

$$\begin{pmatrix} u^{(\ell)}_k(t) \\ v^{(\ell)}_k(t) \end{pmatrix} = \begin{pmatrix} e^{-i\alpha^{(\ell)}(t)}(1-e^{-2i\epsilon_{k,\ell}t})\sin\vartheta_{k,\ell}\cos\vartheta_{k,\ell} \\ \cos^2\vartheta_{k,\ell} + e^{-2i\epsilon_{k,\ell}t}\sin^2\vartheta_{k,\ell} \end{pmatrix}. \quad (15)$$

III. COMPLEXITY ACROSS NONEQUILIBRIUM QPTs

In this section we discuss the circuit complexity of the instantaneous states (3) using the geometric approach introduced in [13,14]. Namely, we look for the optimal circuit $U = U(t)$ connecting the reference and target states, $|T\rangle = U|R\rangle$, with $|R\rangle = \bigotimes_{k>0}|0_k 0_{-k}\rangle$ and $|T\rangle = |\Psi(t)\rangle$. Note that we choose $|R\rangle$ to be the same as the initial condition $|\Psi(0)\rangle$ so that the complexity starts from a vanishing value at $t = 0$. Factorization of states in fixed-momentum sectors implies that $U = \bigotimes_{k>0} U_k$. In terms of Nambu spinors, each admissible U_k is a Bogoliubov transformation taking the reference spinor $\Psi^R_k = (0\ 1)^\intercal$ to $\Psi^{(\ell)}_k(t) = [u^{(\ell)}_k(t)\ v^{(\ell)}_k(t)]^\intercal$ derived in (15). Since these are $SU(2)$ transformations, it is natural to seek factorized circuits $\mathcal{U}(s) = \bigotimes_{k>0}\mathcal{U}_k(s)$ with each factor having the Hamiltonian form

$$\mathcal{U}_k(s) = \mathcal{P}e^{\int_0^s H_k(s')ds'}, \quad H_k(s') \equiv \sum_I Y^I_k(s')\mathcal{O}_I, \quad (16)$$

where $s \in [0,1]$ is a continuous parameter, the functions $Y^I_k(s) = -\frac{1}{2}\mathrm{Tr}[\partial_s\mathcal{U}_k(s)\mathcal{U}_k(s)^{-1}\mathcal{O}_I]$ identify a particular circuit, $\mathcal{O}_I \in \{i\sigma^x, i\sigma^y, i\sigma^z\}$ are the $\mathfrak{su}(2)$ generators (our fundamental gates), and $\mathcal{P}$ is a path-ordering operator ensuring that the circuit is built from smaller to larger values of s. The boundary conditions $\mathcal{U}_k(s=0) = \mathbb{1}$ and $\mathcal{U}_k(s=1) = U_k$ guarantee that any such circuit implements the desired task of connecting the two given states. The optimal circuit is found by minimizing an associated depth functional, $\mathcal{D}[\mathcal{U}_k] = \int_0^s ds' F(\{Y_k(s')\})$, and the corresponding complexity corresponds to the depth of this optimal circuit,

$$\mathcal{C}[\mathcal{U}_k] = \min_{\{Y^I_k(s)\}} \mathcal{D}[\mathcal{U}_k] = \mathcal{D}\big[\mathcal{U}^{\mathrm{opt}}_k\big]. \quad (17)$$

We choose as the cost function F the Euclidean norm $F(\{Y_k\}) = (\sum_I |Y^I_k|^2)^{1/2}$, which is the simplest one satisfying all the required properties from complexity measures [13] (see [17] for alternatives).

To solve the minimization problem it will be convenient to use the polar representation of the components of (15), namely, $v^{(\ell)}_k(t) \equiv \cos\Theta_{k,\ell}(t)\, e^{i\varphi^v_{k,\ell}(t)}$ and $u^{(\ell)}_k(t) \equiv \sin\Theta_{k,\ell}(t)\, e^{i\varphi^u_{k,\ell}(t)}$, with $0 \leqslant \Theta_{k,\ell}(t) \leqslant \pi/2$, and to further discard a global phase to choose the element in the ray of $\Psi^{(\ell)}_k(t)$ to be

$$\Psi^{(\ell)}_k(t) = \begin{pmatrix} e^{i\beta_{k,\ell}(t)}\sin\Theta_{k,\ell}(t) \\ \cos\Theta_{k,\ell}(t) \end{pmatrix}, \quad (18)$$

with $\beta_{k,\ell}(t) \equiv \varphi^u_{k,\ell}(t) - \varphi^v_{k,\ell}(t)$. The Bogoliubov transformation to be implemented thus assumes the form

$$U_k = \begin{pmatrix} \cos\Theta_{k,\ell}(t) & e^{i\beta_{k,\ell}(t)}\sin\Theta_{k,\ell}(t) \\ -e^{-i\beta_{k,\ell}(t)}\sin\Theta_{k,\ell}(t) & \cos\Theta_{k,\ell}(t) \end{pmatrix}. \quad (19)$$

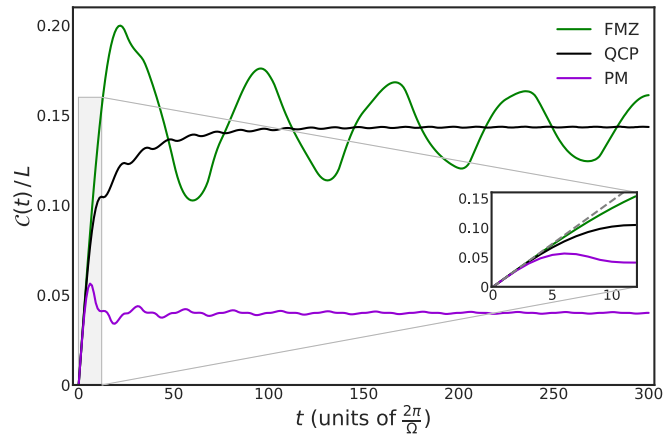

FIG. 2. Time evolution of the complexity (22) near the Ising nonequilibrium transition. The parameters are $L = 1000$, $\ell = 2$, $J = 0.01\Omega$, $g_1 = \Omega$, and varying $\delta g^{(\ell)}_0 = (0, J, 2J)$, corresponding, respectively, to the ferromagnetic phase (FMZ), the quantum critical point (QCP), and the paramagnetic phase (PM). The dashed line in the inset shows the universal linear growth (23) at early times.

This suggests a parametrization of the circuit $\mathcal{U}_k(s) \in SU(2)$ for each momentum sector k in terms of Hopf coordinates (ϕ_1, ϕ_2, ω),

$$\mathcal{U}_k(s) = \begin{pmatrix} e^{i\phi_1(s)}\cos\omega(s) & e^{i\phi_2(s)}\sin\omega(s) \\ -e^{-i\phi_2(s)}\sin\omega(s) & e^{-i\phi_1(s)}\cos\omega(s) \end{pmatrix}. \quad (20)$$

With this at hand, it is straightforward to show that the optimal circuit minimizes the functional

$$\mathcal{D}[\mathcal{U}_k] = \int_0^1 ds' \sqrt{\omega'^2 + \cos^2\omega\,\phi_1'^2 + \sin^2\omega\,\phi_2'^2}. \quad (21)$$

The minimum corresponds to constant phase functions $\phi_1(s) = \phi^0_1$, $\phi_2(s) = \phi^0_2$ and the linear profile $\omega(s) = \omega_0 + s\,\omega_1$, which immediately implies $\mathcal{D}[\mathcal{U}^{\mathrm{opt}}_k] = |\omega_1|$. The boundary condition at $s = 0$ then fixes $\phi^0_1 = 0$ and $\omega_0 = 0$, while the one at $s = 1$ fixes $\omega_1 = \Theta_{k,\ell}(t)$ and $\phi^0_2 = \beta_{k,\ell}(t)$, which fully determines $\mathcal{C}[\mathcal{U}_k]$ defined in (17). After summing over all momentum sectors, we obtain the circuit complexity $\mathcal{C}(t) = \sum_{k>0}|\Theta_{k,\ell}(t)|$, or, explicitly,

$$\mathcal{C}(t) = \sum_{k>0}\left|\arcsin\left(\frac{\Delta_k\gamma^{(\ell)}}{\epsilon_{k,\ell}}\sin(\epsilon_{k,\ell}t)\right)\right|. \quad (22)$$

The full time evolution of $\mathcal{C}(t)$ is depicted in Fig. 2 for the Ising-like nonequilibrium QPT controlled by g_0. The early time behavior is readily obtained by a series expansion of (22), with the summation over momenta performed analytically for the leading term, yielding

$$\mathcal{C}(t \to 0) = \frac{2J\,|\gamma^{(\ell)}|}{\sin\frac{\pi}{L}}\,t + \mathcal{O}(t^3). \quad (23)$$

Note that in the thermodynamic limit $L \to \infty$ one has a volume law, $\mathcal{C} \sim L$. Interestingly, the linear growth at early times is independent of the constant field g_0. The inset in Fig. 2 shows this universal early time behavior, which can be estimated to hold up to a timescale $t_*(g_0) \sim \min_k |2\delta g^{(\ell)}_0 - \omega_k|^{-1} \approx |2|g_0 - g^{(\ell)}_0| + 2J|^{-1}$.

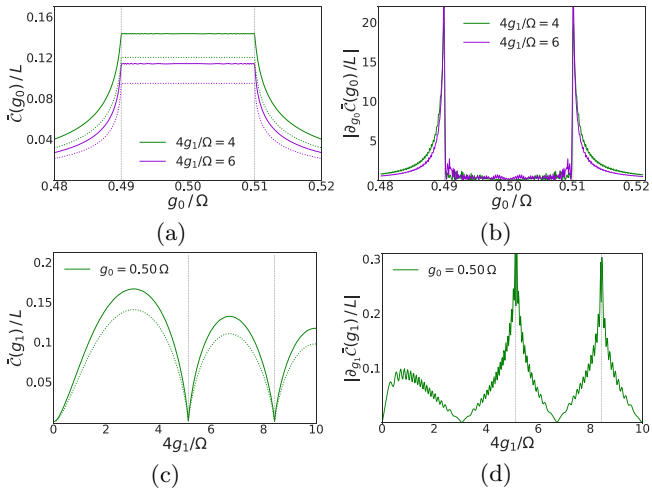

FIG. 3. Time-averaged complexity $\overline{\mathcal{C}}$ over $T = 1000$ periods and its derivatives for $\ell = 2$, $\Omega = \pi$, $J = 0.01\Omega$, $L = 1000$. (a) $\overline{\mathcal{C}}$ close to the Ising QPT for two values of g_1; the dotted lines show the corresponding Floquet mode complexity $\mathcal{C}^-$. (b) Singular behavior of the first derivative of $\overline{\mathcal{C}}$ at the QPT points. (c) and (d) repeat the analysis of (a) and (b) for the first two anisotropic QPT points.

The complexity clearly distinguishes between the two phases and the critical point—in particular, it never equilibrates for g_0 in the FMZ phase. In the PM phase, it reaches the steady value $\mathcal{C}_\infty^{\rm PM}$ more rapidly for increasing g_0, as one can infer from $t_*(g_0)$ estimated above and confirm numerically. Note that $\mathcal{C}_\infty^{\rm PM}$ is bounded from above by the value at the critical point $\mathcal{C}_\infty^{\rm QCP}$, and in particular, it decreases as g_0 grows. Physically, this is an expression of the disordered character of the PM phase: complex (i.e., nonlocal) operations are required to create order in a state prepared on it, while simple (local) operations, like a phase shift, would maintain the disorder of such a state. When g_0 is large, the effect of the driving field is suppressed and does not favor the possibility of creating operators complex enough to order the system, keeping it close to the initial paramagnetic ground state.

The critical behavior becomes more evident in terms of the time-averaged complexity

$$\overline{\mathcal{C}} = \lim_{T\to\infty} \frac{1}{T}\int_0^T dt\, \mathcal{C}(t). \tag{24}$$

This quantity develops a nonanalytic behavior at the quantum critical point, as shown in Fig. 3. Such discontinuity manifests as divergences in the derivatives at the critical points. This critical behavior is reminiscent of the behavior of the complexity in the undriven Ising model, which is discussed in the Appendix.

Independent of g_0, it is evident that the complexity vanishes at the special anisotropic QPT points $\gamma^{(\ell)} = 0$ designed by tuning g_1 and Ω to the Bessel zeros. This is a manifestation of the previously mentioned dynamic localization or CDT phenomenon happening at these points that freezes the quantum dynamics to the initial paramagnetic state. We also note that (22) is symmetric under $\gamma^{(\ell)} \to -\gamma^{(\ell)}$, showing that the complexity is unable to distinguish between the FMY and FMZ phases separated by the CDT point. Near these points, we can check that $\overline{\mathcal{C}} \propto |\gamma^{(\ell)}| \propto |g_1 - g_1^c|$ to first order, which explains the type of nonanalyticity observed in Fig. 3(c). Such behavior is essentially due to the complexity of the Floquet mode Φ^- since in this limit the Bogoliubov angle (11) approaches zero and, therefore, the amplitude for the positive mode in (5), $A^+_{k,\ell} = -\sin\vartheta_{k,\ell}$, vanishes.

In fact, the similarity between $\overline{\mathcal{C}}$ and the complexity of Floquet modes is to be expected on more general grounds. At late times, after transients die out, the system synchronizes with the driving field, and the dynamics is known to be governed by the Floquet modes [33]. Indeed, one can take a step further and make a concrete comparison by explicitly evaluating the complexity for each of the Floquet modes. We first note that those are easily put in the convenient form (25),

$$\begin{aligned}\Phi_k^{+(\ell)}(t) &\simeq \begin{pmatrix} e^{-i\alpha^{(\ell)}(t) - i\pi}\sin\left(\vartheta_{k,\ell} - \frac{\pi}{2}\right) \\ \cos\left(\vartheta_{k,\ell} - \frac{\pi}{2}\right)\end{pmatrix},\\ \Phi_k^{-(\ell)}(t) &\simeq \begin{pmatrix} e^{-i\alpha^{(\ell)}(t)}\sin\vartheta_{k,\ell} \\ \cos\vartheta_{k,\ell}\end{pmatrix},\end{aligned} \tag{25}$$

from which the complexity follows trivially by paralleling the previous calculation and will be constant in time, namely, $\mathcal{C}^+ = \sum_{k>0}|\vartheta_{k,\ell} - \frac{\pi}{2}|$ and $\mathcal{C}^- = \sum_{k>0}|\vartheta_{k,\ell}|$. When $t \to \infty$, we expect that the $e^{-2i\epsilon_{k,\ell}t}$ oscillations in (15) result in small contributions to the time-averaged complexity due to destructive interference (the same cannot be said about the $e^{-i\alpha^{(\ell)}(t)}$ prefactor, which contains the resonant term that survives to wild oscillations), so that the main contributions to $\overline{\mathcal{C}}$ come from the Floquet state $\Phi_k^{-(\ell)}(t)$. In other words, $\mathcal{C}(t\to\infty) \sim \mathcal{C}^-$, and as consequence, the time average $\overline{\mathcal{C}}$ should replicate the behavior of $\mathcal{C}^-$, as is, indeed, seen in Figs. 3(a) and 3(c).

IV. FINAL REMARKS

We have studied the Floquet dynamics of Nielsen's circuit complexity for the Ising model driven by a time-periodic transverse field. At high enough driving frequency, the model is analytically tractable and admits an exact determination of the nonequilibrium phase transitions induced by the external field. Here we showed that the complexity is able to diagnose these nonequilibrium QPTs, extending previous ideas in the literature for quantum quench protocols and hence strengthening the case for complexity as a tool to understand the nonequilibrium physics of many-body systems. In particular, we showed that for a paramagnetic reference state, the complexity of the instantaneous time-evolved state can only equilibrate at large times provided the critical point is not crossed; otherwise, it oscillates indefinitely in time. We also proved that the early time transient behavior of the complexity is linear and independent of the constant driving field g_0 up to a timescale inversely proportional to g_0. The long-time average of the complexity presents nonanalytical behavior at the critical points, which can be traced back to the fact that the asymptotic dynamics is governed by the Floquet modes.

The sensitivity of the circuit complexity to nonequilibrium critical phenomena encourages us to investigate its role in the description of dynamical phase transitions [46], which are characterized by a nonanalytical behavior in the time domain and whose scaling and universality properties are not fully

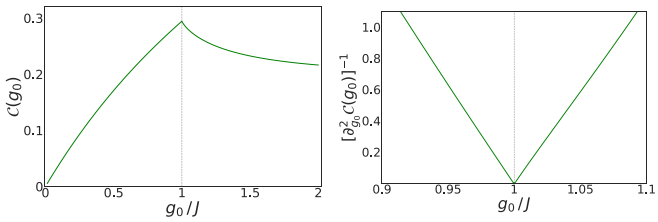

(a) (b)

FIG. 4. (a) Complexity of the ground state of the undriven Ising model with $J = 1$. (b) $|g_0 - J|^{-1}$ behavior of the second derivative near the critical point.

understood. These phenomena can be engineered using quantum quenches or in periodically driven systems similar to the one studied here [47]. The time evolution of complexity (the analog of Fig. 2) should develop a singular behavior at the critical time t_c and may help in the classification of nontrivial topological Floquet phases. This work is in progress.

Another interesting future direction to pursue would be to see how the present analysis generalizes to the case of interacting models, where gates more elaborate than the simple $SU(2)$ rotations used here are required to produce physically interesting states. Here the set of integrable spin chains immediately comes to mind [48]. A more ambitious goal would be the study of a many-body localization/thermal transition, which can be modeled with a Floquet system with no conserved charges [49].

ACKNOWLEDGMENTS

We are grateful to S. Ëliens and D. Trancanelli for discussions and comments. G.C. thanks MEC and MCTIC for financial support. The work of D.T. was supported by FAPESP Grant No. 2017/02300-2.

APPENDIX: COMPLEXITY IN THE ISING MODEL

In order to further illustrate how the circuit complexity can be used to diagnose an equilibrium QPT as well, let us evaluate it for the standard Ising model with a constant transverse field. We take both reference and target states belonging to the ground state manifold; that is, they can be written as $(\cos\eta_k^{(\mathrm{R,T})} + i\sin\eta_k^{(\mathrm{R,T})})^{\otimes k>0}|0\rangle$, such that the complexity assumes the simple form $\mathcal{C} = \sum_k |\Delta\eta_k|$, where $\Delta\eta_k$ is the relative Bogoliubov angle between $|R\rangle$ and $|T\rangle$. Here it is straightforward to work even in the infinite chain limit, where

$$\mathcal{C} = \frac{1}{2\pi}\int_0^\pi dk\,|\Delta\eta_k|. \tag{A1}$$

Using the usual spectrum and Bogoliubov angle of the Ising model, one can easily compute this object, which is illustrated in Fig. 4, where, for simplicity, we have chosen $\eta_k^{(\mathrm{R})} = 0$. The first derivative is discontinuous at the quantum critical point, $g_0 = J$, while the second derivative diverges with a unit critical exponent, that is, $\sim|g_0 - J|^{-1}$, as shown in Fig. 4(b).

[1] T. Kibble, J. Phys. A **9**, 1387 (1976).
[2] W. Zurek, Nature (London) **317**, 505 (1985).
[3] J. Dziarmaga, Phys. Rev. Lett. **95**, 245701 (2005).
[4] A. Polkovnikov, Phys. Rev. B **72**, 161201(R) (2005).
[5] W. H. Zurek, U. Dorner, and P. Zoller, Phys. Rev. Lett. **95**, 105701 (2005).
[6] S.-J. GU, Int. J. Mod. Phys. B **24**, 4371 (2010).
[7] A. Osterloh, L. Amico, G. Falci, and R. Fazio, Nature **416**, 608 (2002).
[8] G. Vidal, J. I. Latorre, E. Rico, and A. Kitaev, Phys. Rev. Lett. **90**, 227902 (2003).
[9] B. Zeng, X. Chen, D.-L. Zhou, and X.-G. Wen, *Quantum Information Meets Quantum Matter: From Quantum Entanglement to Topological Phases of Many-Body Systems* (Springer-Verlag, New York, 2019).
[10] F. Liu, S. Whitsitt, J. B. Curtis, R. Lundgren, P. Titum, Z.-C. Yang, J. R. Garrison, and A. V. Gorshkov, Phys. Rev. Research **2**, 013323 (2020).
[11] Z. Xiong, D.-X. Yao, and Z. Yan, Phys. Rev. B **101**, 174305 (2020).
[12] N. Jaiswal, M. Gautam, and T. Sarkar, arXiv:2005.03532.
[13] M. A. Nielsen, arXiv:quant-ph/0502070.
[14] M. A. Nielsen, Science **311**, 1133 (2006).
[15] D. Stanford and L. Susskind, Phys. Rev. D **90**, 126007 (2014).
[16] A. R. Brown, D. A. Roberts, L. Susskind, B. Swingle, and Y. Zhao, Phys. Rev. Lett. **116**, 191301 (2016).
[17] R. Jefferson and R. C. Myers, J. High Energy Phys. 10 (2017) 107.
[18] P. Caputa and J. M. Magan, Phys. Rev. Lett. **122**, 231302 (2019).
[19] V. Balasubramanian, M. Decross, A. Kar, and O. Parrikar, J. High Energy Phys. 01 (2020) 134.
[20] A. Polkovnikov, K. Sengupta, A. Silva, and M. Vengalattore, Rev. Mod. Phys. **83**, 863 (2011).
[21] A. Mitra, Annu. Rev. Condens. Matter Phys. **9**, 245 (2018).
[22] D. W. Alves and G. Camilo, J. High Energy Phys. 06 (2018) 029.
[23] H. A. Camargo, P. Caputa, D. Das, M. P. Heller, and R. Jefferson, Phys. Rev. Lett. **122**, 081601 (2019).
[24] S. Liu, J. High Energy Phys. 07 (2019) 104.
[25] T. Ali, A. Bhattacharyya, S. S. Haque, E. H. Kim, and N. Moynihan, arXiv:1811.05985.
[26] A. Eckardt, Rev. Mod. Phys. **89**, 011004 (2017).
[27] T. Oka and S. Kitamura, Annu. Rev. Condens. Matter Phys. **10**, 387 (2019).
[28] H. Lignier, C. Sias, D. Ciampini, Y. Singh, A. Zenesini, O. Morsch, and E. Arimondo, Phys. Rev. Lett. **99**, 220403 (2007).
[29] N. H. Lindner, G. Refael, and V. Galitski, Nat. Phys. **7**, 490 (2011).
[30] G. Jotzu, M. Messer, R. Desbuquois, M. Lebrat, T. Uehlinger, D. Greif, and T. Esslinger, Nature (London) **515**, 237–240 (2014).

[31] V. Mukherjee and A. Dutta, J. Stat. Mech. (2009) P05005.
[32] A. Das, Phys. Rev. B **82**, 172402 (2010).
[33] A. Russomanno, A. Silva, and G. E. Santoro, Phys. Rev. Lett. **109**, 257201 (2012).
[34] V. M. Bastidas, C. Emary, G. Schaller, and T. Brandes, Phys. Rev. A **86**, 063627 (2012).
[35] D. H. Dunlap and V. M. Kenkre, Phys. Rev. B **34**, 3625 (1986).
[36] F. Grossmann, T. Dittrich, P. Jung, and P. Hänggi, Phys. Rev. Lett. **67**, 516 (1991).
[37] E. Kierig, U. Schnorrberger, A. Schietinger, J. Tomkovic, and M. K. Oberthaler, Phys. Rev. Lett. **100**, 190405 (2008).
[38] A. Eckardt, C. Weiss, and M. Holthaus, Phys. Rev. Lett. **95**, 260404 (2005).
[39] M. Sillanpää, T. Lehtinen, A. Paila, Y. Makhlin, and P. Hakonen, Phys. Rev. Lett. **96**, 187002 (2006).
[40] E. Lieb, T. Schultz, and D. Mattis, Ann. Phys. (NY) **16**, 407 (1961).
[41] S. Bhattacharyya, A. Das, and S. Dasgupta, Phys. Rev. B **86**, 054410 (2012).
[42] S. Ashhab, J. R. Johansson, A. M. Zagoskin, and F. Nori, Phys. Rev. A **75**, 063414 (2007).
[43] Q. Xie and W. Hai, Phys. Rev. A **82**, 032117 (2010).
[44] T. Mikami, S. Kitamura, K. Yasuda, N. Tsuji, T. Oka, and H. Aoki, Phys. Rev. B **93**, 144307 (2016).
[45] E. Barouch, B. M. McCoy, and M. Dresden, Phys. Rev. A **2**, 1075 (1970).
[46] M. Heyl, Rep. Prog. Phys. **81**, 054001 (2018).
[47] K. Yang, L. Zhou, W. Ma, X. Kong, P. Wang, X. Qin, X. Rong, Y. Wang, F. Shi, J. Gong *et al.*, Phys. Rev. B **100**, 085308 (2019).
[48] V. Gritsev and A. Polkovnikov, SciPost Phys. **2**, 021 (2017).
[49] L. Zhang, V. Khemani, and D. A. Huse, Phys. Rev. B **94**, 224202 (2016).